

# DEVELOPMENT OF A MULTISEGMENTED, QUASI-STATIC CABLE MODEL WITH AN ANALYTICAL JACOBIAN FOR MODELING FLOATING OFFSHORE WIND TURBINES\*

MARCO MASCIOLA<sup>†</sup> AND JASON JONKMAN<sup>‡</sup>

**Abstract.** Multisegmented mooring lines have widespread, practical utility in realistic offshore anchoring designs. As such, the modeling tools used to design these systems should represent the properties accurately, such as the variable stiffness and mass properties along the line and line-to-line interconnections. The conventional approach used for solving a multisegmented static mooring system relies on a partitioned algorithmic: equations describing the system physics are solved individually and with nested root-finding algorithms. This method requires a component Jacobian to be computed with finite-difference because closed-form derivatives of the force-balance terms cannot be obtained. A new method to compute the mooring line geometry and forces in multisegmented systems is proposed in this paper. Unlike the traditional partitioned approach, the proposed method approaches the problem monolithically, thereby allowing the entire Jacobian structure to be computed analytically using a single-level solver. However, like most coupled problems, this method is prone to ill-conditioning. An understanding of the Jacobian structure is necessary before sensitivities of the solution can be addressed. The ability to include seabed contact, seabed friction, and externally applied forces at the line interconnection points are other novel features of this model.

**Key words.** quasi-static, mooring, static analysis, cable, floating offshore wind turbine

<b>Symbol</b>	<b>Description</b>
$A$	Cable cross-sectional area
$C_B$	Seabed contact friction coefficient
$B_j$	Displaced volume at the $j^{\text{th}}$ node
$E$	Cable Young's modulus
$\mathcal{F}_0$	Global reference frame origin
$\mathcal{F}_i$	$i^{\text{th}}$ local reference frame attached to element $i$
$F_{X_j, Y_j, Z_j}^{\text{ext}}$	External force applied to the $j^{\text{th}}$ node
$g$	Acceleration due to gravity
$h$	Vertical fairlead excursion
$H$	Horizontal fairlead force
$H_A$	Horizontal anchor force
$l$	Horizontal fairlead excursion
$L$	Unstretched line length
$L_B$	Line length resting on the seabed
$M_j$	Point mass applied to the $j^{\text{th}}$ node
$\mathbf{r}_i$	Node position vector $[x_i, y_i, z_i]$
$s$	Unstretched distance from the anchor ( $0 \leq s \leq L$ )
$\mathbf{T}_i$	Cable tension vector $[H_i, V_i]$
$T_e(s)$	Cable tangential tension at distance $s$
$\mathbf{u}$	Input state vector
$V$	Vertical fairlead force
$V_A$	Vertical anchor force
$x_0$	Horizontal force transition point for $H(s) > 0$

---

\*This work was supported by the U.S. Department of Energy Offshore Wind and Water Power Program.

<sup>†</sup>Postdoctoral Researcher, National Renewable Energy Laboratory, Golden, Colorado (marco.masciola@nrel.gov).

<sup>‡</sup>Senior Engineer, National Renewable Energy Laboratory, Golden, Colorado.

$\mathbf{z}$	Constraint state vector
$\mathbf{Z}_R$	Residual vector
$\alpha_i$	Rotation angle between the $x_i$ and $X$ axis
$\rho$	Fluid density
$\rho_{\text{cable}}$	Cable density
$\omega$	Cable weight per unit length in fluid

**1. Introduction.** The utility of cable-supported systems have been manifested throughout the course of history, and a background account of the various structures utilizing cable systems is well documented in [19]. In large systems, such as bridges and offshore wind platforms, cables offer a lightweight option to support the system weight. In shallow water offshore wind installations, fixed-bottom support structures, such as jacket structures, are the preferred choice. As water depth increases, the design becomes less economical since more steel is required to support the structure. In deeper waters, floating platforms have an economic advantage, and are aided by the use of mooring lines to steadily position the system. The overall objective of reducing the amount of steel used in the structure is achieved with this strategy, thereby making wind resources in deep waters accessible. There is a push to deploy wind turbines offshore because there is an abundant supply of offshore wind resource in close proximity to dense population centers. However, offshore wind economics favors larger devices, and new technologies must be developed to meet the requirements of the unforgiving offshore conditions [25]. One strategy to reduce cost is to develop novel and cost-saving station-keeping and anchoring methods that meet the unique need of floating offshore wind turbines.

Mooring models used for simulating floating offshore wind systems can be classified into two groups: static models and dynamic models. Static models ignore the inertia forces and fluid drag loads, and only account for the mean forces in the mooring system, including elasticity, weight (in fluid), and geometric nonlinearities. Although these limitation are acknowledged, static models are an integral component of the initial design and analysis phase. The advantage of static models concerns computational efficiency, in that they can arrive at solutions quickly (but at the cost of reduced model fidelity). As a step towards achieving this goal, a new method to solve a network of interconnected cables held in static equilibrium is proposed. The generic term for this system of interconnected cables is referred to as ‘multisegment’, and one application of this systems is visualized in Figure 1. Bridle mooring systems, as demonstrated in Figure 2, are often times invoked in the design to increase the stiffness in a direction to accommodate environmental loads. In the case of the spar platform in Figure 1, the vessel yaw stiffness is increased (rotation about the vertical  $z$ -axis). Other offshore applications for multisegment cables are also offered in [5, 13, 8]. The multisegment theory introduced in this manuscript is also useful outside of bridle mooring designs, such as modeling a single line with non-homogeneous properties along its length. Most deep water mooring designs involve systems with sections of the line composed of different materials connected together in series [5]\*. The essence of the strategy is to replace the heaviest portion of the line with a lightweight material to decrease strain due to self-weight, which is important as water depth increases.

Although the system analyzed in this manuscript concerns mooring systems for floating offshore wind turbines, the technique can be extended to other geometrically nonlinear cable systems, including tensegrity systems [33], cable actuated robots [18,

---

\*One such common application is chain-wire rope-chain.

2], bridges [30], and tethered airships [37]. Floating offshore systems, such as floating wind turbines [32, 35] and oil and gas production platforms [1], are largely supported in station-keeping operations using permanent mooring designs [3, 4].



FIG. 1. *The spar platform pictured illustrates a practical use for a multisegmented line in floating offshore wind turbines. The bridle joint provides additional yaw stiffness, an essential component for dynamic stability.*

**1.1. Conventional Quasi-Static Strategies.** The process of applying a static cable model in a dynamic simulation is often referred to as ‘*quasi-static*’ analysis. The premise of the approach is to incrementally adjust the fairlead position based on the vessel displacements, and re-solve the algebraic equations describing the cable geometry to extract the force variables. By knowing the cable anchor and fairlead locations, the cable geometry and internal tensions can be obtained. Unlike the dynamic models offered in [12] and [9], quasi-static models fail to capture effects driven by cable inertia. Ignoring inertia can lead to an under-prediction of the extreme line tensions and vessel offsets [23]. Although this limitation is acknowledged, quasi-static models are viewed as an acceptable surrogate in lieu of dynamic analysis since the mean mooring line forces are preserved by quasi-static models [3]. The underlying difference in quasi-static analysis is that algebraic equations are solved, whereas integration of the equation of motion occurs with dynamic cable models.

Quasi-static models can appear in several forms. The common and most widely-used approach barrows the continuous analytical equation as demonstrated by [27] and [19]. These closed-form analytical models account for cable stretch and sag due to self weight, assume homogeneous properties along the line, and ignore effects from

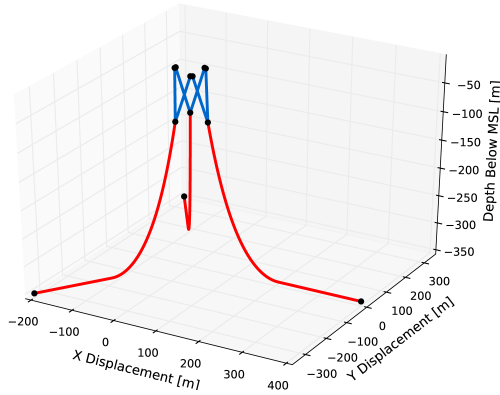


FIG. 2. Illustration of an example multisegmented system solved using the techniques defined in this manuscript. The ability to model cable/seabed contact analytically is a unique feature of this model.

bending, torsion, shear and drag. A second quasi-static analysis method is to use a discretized chain of elastic elements to model the system [7, 21]. This technique improves over the conventional continuous analytical approach since fluid drag forces and irregular (inclined) seabed boundaries can be represented; however, solving the algebraic equations for the discretized system can become more costly than performing the integration for the dynamic model [36].

Traditional multisegmented methods for analytical models, such as those proposed in [28], invoke partitioned (nested) solvers. Because the solution to the catenary is unique [34], convergence towards the global solution is guaranteed for the single line case. This hierarchical solve strategy is sufficient to find the solution, as is evident by the recent work in [29]. In the influential work proposed by [28], the solution strategy relies on finite-differencing to compute the Jacobian. [28] recommend introducing numerical damping to encourage stability and to decreased the rate of change in the solution between subsequent iterations. In [15], the continuous model in [19] was adapted to account for cable-seabed contact; however, this model was introduced for single-line elements only. The multisegmented, quasi-static cable model developed in this manuscript will focus on the single-line, continuous analytical models offered in [19] and [15], and will extend it for multi-element systems, but without a partitioned solver.

**1.2. Unique Features of the Proposed MSQS Model.** The multisegmented, quasi-static (MSQS) cable model developed in this manuscript is adapted to be a component of the Mooring Analysis Program (MAP). MAP is an open-source program developed to simulate the nonlinear restoring force in marine cables and is envisioned to contain multiple mooring models, both quasi-static and dynamic. This paper will focus on developing the theory driving the MSQS model. MAP is developed as an independent library for the FAST wind turbine simulation program [14]. FAST was recently re-written into a new modular format to take advantage of the updated Fortran standards [17, 16], to streamline the integration of customized third-party modules into the driver program and to permit various levels of modeling fidelity, multiple coupling approaches, and state linearization. The subroutine calling convention directed by the FAST modularized framework functions as a basis for interacting with MAP's MSQS model: the entry points for modifying the system properties, up-

dating parameters, and executing the solve steps can be redefined in any particular order to suit the needs of an application.

The unique features of the MSQS model include:

1. The ability to select mooring line geometry at run-time.
2. The ability to lump a point mass, buoyancy module, and other external force at nodes.
3. The Jacobian matrix is computed analytically rather than through finite-difference.
4. The problem is treated in a monolithic fashion. Previous endeavors has resorted to separating the different physics and solving them in a partitioned approach.
5. The inclusion of a close-form, continuous analytical solution to the cable-seabed contact problem.
6. Integration of the MSQS model into the FAST modularized framework [16].

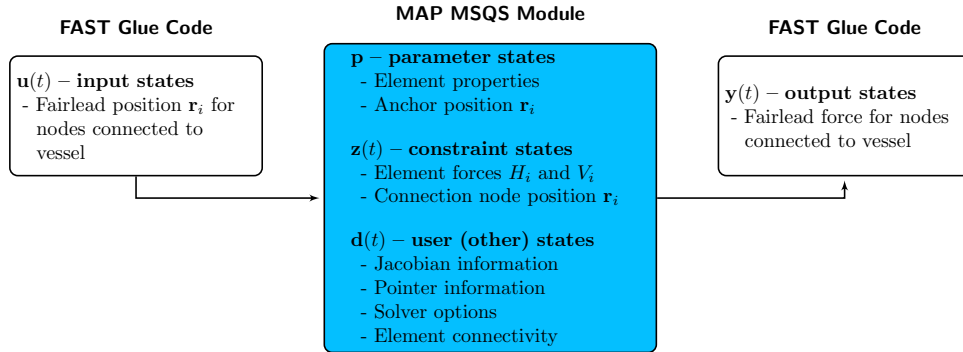


FIG. 3. Organization of the MAP states within the construction of the FAST framework for loose coupling.

Items 2–6 will be explored in this manuscript. Readers are referred to the earlier work found in [22] for details regarding item 1 above. The MSQS model is viewed as a precursor to the eventual development of a discretized dynamic cable model that will be included within the MAP suite of tools. Both the MSQS model and dynamic mooring models are viewed as a network of nodes and elements, and the principle differences driving the solution are the equations operating on the nodes and elements. In principle, the system being solved in this application can also be done using the approach found in [28], but is different because 1) the problem is treated as a coupled multi-physics systems, 2) the Jacobian is achieved analytically, 3) geometries are selected at run-time, and 4) seabed contact is incorporated into the solution.

**1.3. FAST Framework Taxonomy.** As FAST framework vernacular is used throughout this manuscript, definitions of the different states constituting the FAST framework are provided here. The framework was developed to standardize variable organization, function calling convention, and communication between modules. This framework allows for a wide range of coupling strategies; however, this manuscript defines the MSQS integration in loose coupling terms. FAST is a time-domain, simulation tool composed of multiple modules that combine together to form a compre-

hensive model of a floating offshore wind turbine. The effects included in FAST are attributed to the aerodynamics, control, wind turbine structural dynamics, floating platform hydrodynamics, and mooring restoring forces (as provided by MAP’s MSQS model). The loose coupling strategy illustrated Figure 3 shows the organization of various states and their respective update stages. The inputs,  $\mathbf{u}(t)$ , are fed into the MSQS model by the FAST glue code at each time step  $t$ . Inside the MAP module, the constraint states,  $\mathbf{z}(t)$ , are iterated until the residual function,  $\mathbf{Z}_R$ , are solved. The residual functions are the equations resulting in zero sum-forces in the mooring line connection points. Once the equations are solved such that  $\mathbf{Z}_R = 0$ , the mooring fairlead forces are then passed to the FAST glue code, the equations of motion for the other components of the floating wind system are solved, and the simulation advances to the next time step. Tight coupling is viewed as an extension of loose coupling principles requiring Jacobian information to be passed across the FAST/MAP module barrier and exposure of  $\mathbf{z}(t)$  to the FAST glue code; more information is available in [17] and [16] for an explanation of tight coupling principles.

The rationale behind this architecture in the context of the MSQS model is as follows: once variables are updated in  $\mathbf{u}(t)$  (the inputs), the position of all vessel-attached nodes are updated. The statics solution can then be solved for the updated mooring line geometry by iterating on  $\mathbf{z}(t)$  such that  $\mathbf{Z}_R$  is minimized. Once successfully solved, the newly determined outputs are updated in  $\mathbf{y}(t)$ . The user states data structure is employed internally in the MAP module and understood to contain information pertaining to node-element connectivity and Jacobian non-zero pattern (which is assembled and defined once at run-time initialization). For modules adhering to the NWTC framework, vigilance must be exercised to ensure variables do not simultaneously function as a component of multiple types. The Cable properties, nodes, elements, and connection between node and elements are the essential building blocks for the creation of a multisegmented systems. A dichotomy exists between nodes and elements, Figures 4~5. A change in the node position will influence the element profile, which in effect alters the element line forces. Elements contain system structural properties and geometry, while nodes define the forces acting on the system between mooring line fairleads and anchors.

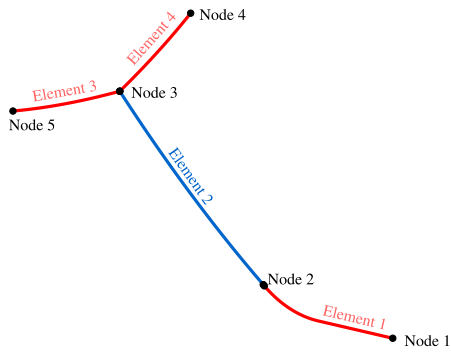


FIG. 4. Definition of the entities constituting a multisegmented mooring system. Elements define line properties, and nodes define connection points between lines and location where external forces are applied.

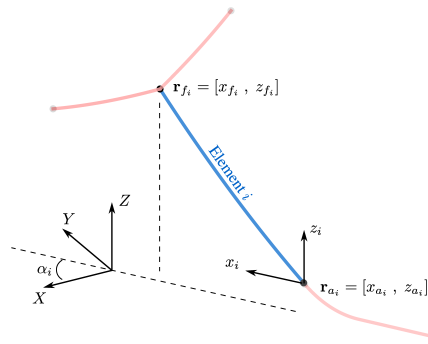


FIG. 5. Notation of the various entities needed in defining the relationship between multiple members in a multisegmented mooring line. The capital letters  $\{X, Y, Z\}$  represent position in the global  $\mathcal{F}_0$  reference frame.



**2. Continuous Analytical Cable Models.** An overview of the equations that need to be solved will be presented prior to explaining the solution technique employed in MAP's MSQS solver. The basis of the approach used in [28] is then explained. From this discussion, the basic principles used in the MSQS model will then be extrapolated.

**2.1. Single-Line Catenary Equation.** The equations used to describe the shape of a suspended chain illustrated in Figure 6 have been derived in numerous works [19, 38]. For completeness, a summary of the governing equations used inside the MSQS model are presented. Given a set of line properties, the line geometry can be expressed as a function of the forces exerted at the end of the line:

$$(2.1a) \quad x(s) = \frac{H}{\omega} \left\{ \ln \left[ \frac{V_a + \omega s}{H} + \sqrt{1 + \left( \frac{V_a + \omega s}{H} \right)^2} \right] - \ln \left[ \frac{V_a}{H} + \sqrt{1 + \left( \frac{V_a}{H} \right)^2} \right] \right\} + \frac{Hs}{EA}$$

$$(2.1b) \quad z(s) = \frac{H}{\omega} \left[ \sqrt{1 + \left( \frac{V_a + \omega s}{H} \right)^2} - \sqrt{1 + \left( \frac{V_a}{H} \right)^2} \right] + \frac{1}{EA} \left( V_a s + \frac{\omega s^2}{2} \right)$$

where:

$$(2.2) \quad \omega = gA(\rho_{\text{cable}} - \rho)$$

and  $x$  and  $z$  are coordinate axes in the local (element) frame, Figure 5. The following substitution can be made for  $V_a$  in the above equations:

$$(2.3a) \quad H_a = H$$

$$(2.3b) \quad V_a = V - \omega L$$

which simply states the decrease in the vertical anchor force component is proportional to the mass of the suspended line. Equations 2.1a~2.1b both describe the catenary profile provided all entries on the right side of the equations are known. However, in practice, the force terms  $H$  and  $V$  are sought, and the known entity is the fairlead excursion dimensions,  $l$  and  $h$ . In this case, the forces  $H$  and  $V$  are found by simultaneously solving the following two equations:

$$(2.4a) \quad l = \frac{H}{\omega} \left[ \ln \left( \frac{V}{H} + \sqrt{1 + \left( \frac{V}{H} \right)^2} \right) - \ln \left( \frac{V - \omega L}{H} + \sqrt{1 + \left( \frac{V - \omega L}{H} \right)^2} \right) \right] + \frac{HL}{EA}$$

$$(2.4b) \quad h = \frac{H}{\omega} \left[ \sqrt{1 + \left( \frac{V}{H} \right)^2} - \sqrt{1 + \left( \frac{V - \omega L}{H} \right)^2} \right] + \frac{1}{EA} \left( VL - \frac{\omega L^2}{2} \right)$$



Lastly, the tension in the line is determined using the following relationship:

$$(2.5) \quad T_e(s) = \sqrt{H^2 + (V_a + \omega s)^2}$$

As outlined previously, Eqs. 2.1a~2.5 are applicable to the case of a cable suspending freely in a fluid and connected to the seabed at the anchor point. This condition is determined by virtue of Eq. 2.3b, which indicates that a catenary must be supported by a force greater than its submerged weight for no line to be resting on the seabed:

$$(2.6) \quad V - \omega L > 0$$

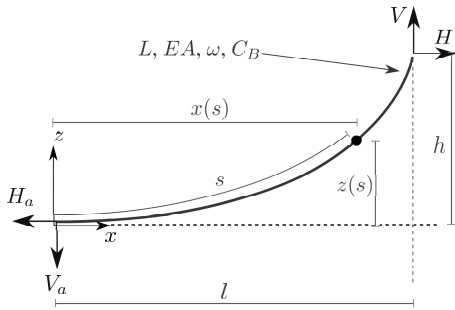


FIG. 6. Definition of parameters used to construct a single line cable element suspended in fluid and anchored to the seabed.

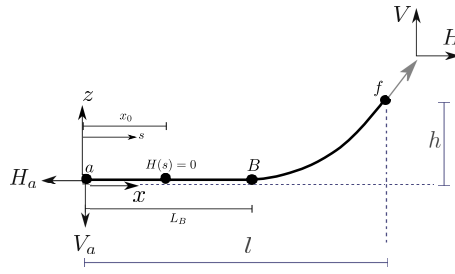


FIG. 7. Definition of parameters used to construct a single line cable element. This image is an adaptation of Figure 6 for the case of a cable resting on the seabed.

**2.2. Single-Line Catenary Equation with Seabed Contact.** The origin of the equations describing a cable resting on the seabed follows a similar derivation process for the suspended case as described in [19]. A free-body diagram for an infinitesimal section of cable resting on the seabed is given in Figure 8. The following assumptions are observed in this derivation:

- Effects from bending, torsion, and shear stiffness are neglected.
- Mass, elastic and cross-sectional properties along the line are constant.
- The seabed contact friction force is directed tangential to the element and only exists on the portion of line resting on the seabed.
- The seabed is perfectly horizontal (not inclined).
- The cable touch-down point is noted as  $B$  in Figure 7.
- The entire cable (on the seabed and hanging in the fluid) lies in a vertical plane. Transverse seabed friction is neglected.

Figure 7 is dissected into three segments. Points  $a$  (the anchor position) and  $f$  (the fairlead position) are typically known entities. The touch-down point  $B$  that is a parameter that is calculated in the course of determining  $H$  and  $V$ , and the displacement  $x_0$  identifies the transition point where  $H(x_0 + \epsilon) > 0$  and  $H(x_0 - \epsilon) = 0$ .  $x_0$  may not exist for all lines, and  $0 \leq H_a$ . This implies that  $x_0 < 0$ , and  $s$  is defined between 0 and  $L$  for this case. The length of line resting on the seabed,  $L_B$ , is a linear function proportional to the vertical force  $V$  magnitude. If the vertical force is not sufficient to suspend the cable, then  $V < \omega L$ , which implies a portion of the

line rests on the seabed. The difference between  $V$  and  $\omega L$  must be accounted for by cable resting on the seabed. This is recognized with the following expression:

$$(2.7) \quad L_B = L - \frac{V}{\omega}$$

When  $L_B > 0$ , then Eq. 2.3b is violated, and the line is no longer fully suspended. Although  $L_B$  is useful in describing the mooring line geometry and juncture of the touch-down point, it is an essential component for determining the transition point  $x_0$ , which is necessary to advance towards the final solution. Because the line is in static equilibrium, the horizontal forces on the line due to friction must equate to the horizontal applied force at the fairlead:

$$(2.8) \quad H = C_B \omega (L_B - x_0)$$

Equation 2.8 is re-casted in the following form for convenience:

$$(2.9) \quad x_0 = L_B - \frac{H}{C_B \omega}$$

With the fundamental geometric components defined, the derivation for the closed-form analytical cable model with seabed contact proceeds by defining the governing differential equations. Through a summation of force in the  $x$  direction, as depicted in Figure 8, one obtains:

$$(2.10) \quad \begin{aligned} \sum F_x = 0 &\Rightarrow H + C_B \omega ds = H + dH \\ &\Rightarrow dH = C_B \omega ds \end{aligned}$$

Next, Hooke's Law is introduced to provide elastic properties in the catenary, leading to the following expression for the tangential tension [38]:

$$(2.11) \quad T_e = EA \left( \frac{dx}{ds} - 1 \right)$$

Because the tension component  $T_e$  is exclusively in the  $x$  direction at the cable/seabed interface, Figure 7, one can make the substitution  $T_e = H$ , allowing Eq. 2.11 to be expressed more conveniently:

$$(2.12) \quad dx = \left( 1 + \frac{H}{EA} \right) ds$$

The next step is to determine the horizontal force  $H(s)$  along the portion touching the seabed. The expression for  $H(s)$  is a prerequisite to determine the equivalent forms of Eqs. 2.1a~2.1b for the cable/seabed contact problem. From Eq. 2.3a, it is inferred that that horizontal force in a suspended line element is constant. This observation exists because the only external force acting on the system is provided by gravity. For the case of a cable resting on the seabed, the rate of change in the element horizontal direction will be proportional to  $C_B \omega$ .

**2.2.1. Horizontal Force.** The horizontal force  $H(s)$  is found by integration Eq. 2.10 from  $a$  to  $B$ , Figure 7.

$$(2.13) \quad \int_{H(s)}^{H_B} dH' = \int_{\text{MAX}(s,x_0)}^{L_B} C_B \omega ds'$$

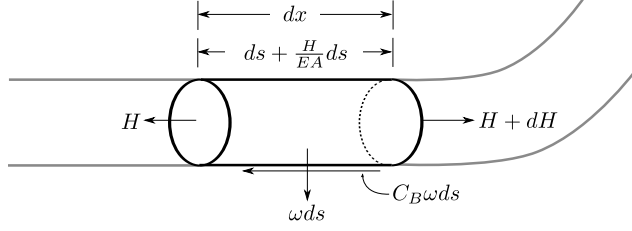


FIG. 8. Free-body diagram for an infinitesimal cable section in contact with the seabed.

where  $s'$  is a dummy variable. The lower limit of integration  $\text{MAX}(s, x_0)$  on the right hand side of Eq. 2.13 echos the minimum distance where  $H(s) > 0$ . In other words, if the tension at  $a$  is zero, then  $x_0$  will be greater. Integrating Eq. 2.13 leads to:

$$(2.14) \quad H_B - H(s) = C_B\omega [L_B - \text{MAX}(s, x_0)]$$

For simplicity,  $H_B = H$  since the  $H$  represents the maximum horizontal tension component in the line, which does not change between points  $B$  and  $f$  (since no external horizontal forces act on the system). This leads to the following expression:

$$(2.15) \quad H(s) = \text{MAX}[H + C_B\omega(s - L_B), H + C_B\omega(x_0 - L_B)]$$

Given Eqs. 2.8 and 2.9, it is apparent one value reduces to zero. The expression for the horizontal then becomes:

$$(2.16) \quad H(s) = \text{MAX}[C_B\omega(s - x_0), 0]$$

**2.2.2. Cable Profile.** The initial step in finding the mooring line profile, which is then used to solve for the horizontal  $H$  and vertical  $V$  fairlead forces, is to first determine the closed-form analytical solution for the line geometry. This is sought by integrating Eq. 2.12.

$$(2.17) \quad \int_0^{x(s)} dx = \int_0^s \left(1 + \frac{H}{EA}\right) ds' \\ = \int_0^s \left\{1 + \frac{\text{MAX}[C_B\omega(s' - x_0), 0]}{EA}\right\} ds'$$

Equation 2.17 leads to two conditional integrals, namely:

$$(2.18) \quad x(s) = \begin{cases} \int_0^s ds' & \text{if } s \leq x_0 \\ \int_0^{\text{MAX}(x_0, 0)} ds' + \int_{\text{MAX}(x_0, 0)}^s \left[1 + \frac{C_B\omega(s' - x_0)}{EA}\right] ds' & \text{if } s > x_0 \end{cases}$$

Equation 2.18 is a valid argument for the section of cable resting on the seabed (i.e., between the range  $0 \leq s \leq L_B$ ). A third argument is included in Eq. 2.18 to account for the section of cable extending beyond point  $B$ . Following through with the integration in Eq. 2.18, it can be shown that  $x(s)$  is equal to:

$$(2.19) \quad x(s) = \begin{cases} s & \text{if } 0 \leq s \leq x_0 \\ s + \frac{C_B\omega}{2EA} [s^2 - 2x_0s + x_0\text{MAX}(x_0, 0)] & \text{if } x_0 < s \leq L_B \\ x_{L_B}^+(s) & \text{if } L_B < s \leq L \end{cases}$$

where  $x_{L_B^+}(s)$  is a yet-to-be introduced quantity. This is found by continuing Eq. 2.1a beyond  $s = L_B$  then adding a constant to ensure continuity of boundary conditions between equations.

$$(2.20) \quad x(s) = \begin{cases} s & \text{if } 0 \leq s \leq x_0 \\ s + \frac{C_B \omega}{2EA} [s^2 - 2x_0 s + x_0 \lambda] & \text{if } x_0 < s \leq L_B \\ L_B + \frac{H}{\omega} \ln \left[ \frac{\omega(s-L_B)}{H} + \sqrt{1 + \left( \frac{\omega(s-L_B)}{H} \right)^2} \right] + \frac{Hs}{EA} + \frac{C_B \omega}{2EA} [x_0 \lambda - L_B^2] & \text{if } L_B < s \leq L \end{cases}$$

where  $\lambda$  is:

$$(2.21) \quad \lambda = \begin{cases} L_B - \frac{H}{C_B \omega} & \text{if } x_0 > 0 \\ 0 & \text{otherwise} \end{cases}$$

The expression  $z(s)$  is found by continuing Eq. 2.1b beyond point  $B$ . Between the range  $0 \leq s \leq L_B$ , the vertical height is zero since the line is resting on the seabed and forces can only occur parallel to the horizontal plane. This produces:

$$(2.22) \quad z(s) = \begin{cases} 0 & \text{if } 0 \leq s \leq L_B \\ \frac{H}{\omega} \left[ \sqrt{1 + \left( \frac{\omega(s-L_B)}{H} \right)^2} - 1 \right] + \frac{\omega(s-L_B)^2}{2EA} & \text{if } L_B < s \leq L \end{cases}$$

Equations 2.20 and 2.22 produce the mooring line profile as a function of  $s$ . Ideally, a closed-form solution for  $l$  and  $h$  is sought to permit simultaneous solves for  $H$  and  $V$ , similar to Eqs. 2.4. This is obtained by substituting  $s = L$  into Eqs. 2.20 and 2.22. This gives:

$$(2.23a) \quad l = L_B + \left( \frac{H}{\omega} \right) \ln \left[ \frac{V}{H} + \sqrt{1 + \left( \frac{V}{H} \right)^2} \right] + \frac{HL}{EA} + \frac{C_B \omega}{2EA} [x_0 \lambda - L_B^2]$$

$$(2.23b) \quad h = \frac{H}{\omega} \left[ \sqrt{1 + \left( \frac{V}{H} \right)^2} - 1 \right] + \frac{V^2}{2EA\omega}$$

Finally, a useful quantity that is often evaluated is the tension as a function of  $s$  along the line. This is given using:

$$(2.24) \quad T_e(s) = \begin{cases} \text{MAX} [H + C_B \omega (s - L_B), 0] & \text{if } 0 \leq s \leq L_B \\ \sqrt{H^2 + [\omega (s - L_B)]^2} & \text{if } L_B < s \leq L \end{cases}$$

The choice of using Eqs. 2.4a~2.4b or Eqs. 2.23a~2.23b is decided by the program depending on the condition of Eq. 2.6; though, run-time flags can be enabled to override this feature so that the classical catenary equations for a suspended line (not in contact with the seabed) can be used.

**3. Multisegmented Strategies.** With the closed-form analytical equations for a single line now derived, two strategies for solving multisegmented problems as illustrated in Figure 2 will be discussed. The first of these methods uses the nested solve technique demonstrated in [28] and [29]. The second of these approaches embraces a monolithic technique employing a single-level root-finder to converge onto the solution. Before discussing the two procedures for solving the system, a kinematic break-down of a multisegmented mooring line is first presented. This vector representation is used to assemble the system connectivity matrix and express the equations to solve this system.

**3.1. Line Kinematics.** With the continuous equations for a single line defined in Eqs. 2.4a~2.4b and 2.23a~2.23b, one can recognize the equations describing the line profile exists in a two-dimensional plane. Because the forces need to be expressed in the three-dimensional  $\mathcal{F}_0$  frame, the two-dimensional equations are converted to a three-dimensional domain. This is initiated by defining a series of  $\mathcal{F}_i$  local frames at the origin in which Eqs. 2.4a~2.4b are written in, Figure 9. Frame  $\mathcal{F}_0$  is an arbitrary global axis, but it is usually observed as the vessel reference origin. Next, introduce vector  $\mathbf{q}(s)$ :

$$(3.1) \quad \mathbf{q}_i(s) = [x_i(s), 0, z_i(s)]^T$$

which defines points along the  $i^{\text{th}}$  line element in the  $\mathcal{F}_i$  local frame. The global position of  $\mathbf{q}_i(s)$  can be procured by the following:

$$(3.2) \quad \mathbf{X}_i(s) = \mathbf{r}_i + \mathbf{R}_i \mathbf{q}_i(s)$$

where  $\mathbf{r}_i$  is the origin of  $\mathcal{F}_i$  relative to  $\mathcal{F}_0$ , and  $\mathbf{R}_i$  is an orthonormal rotation matrix about the vertical ( $Z/z_i$ ) axis:

$$(3.3) \quad \mathbf{R}_i = \begin{bmatrix} \cos \alpha_i & -\sin \alpha_i & 0 \\ \sin \alpha_i & \cos \alpha_i & 0 \\ 0 & 0 & 1 \end{bmatrix}$$

The angle  $\alpha_i$  is determined by the relationship:

$$(3.4) \quad \alpha_i = \cos^{-1} \left[ \frac{(\{\mathbf{r}_{\text{anchor}}\}^{x,y} - \{\mathbf{r}_{\text{fairlead}}\}^{x,y}) \cdot \hat{\mathbf{i}}}{\|\{\mathbf{r}_{\text{anchor}}\}^{x,y} - \{\mathbf{r}_{\text{fairlead}}\}^{x,y}\|} \right]$$

$$= \cos^{-1} \left[ \frac{\{\mathbf{r}_{\text{anchor}}\}^x - \{\mathbf{r}_{\text{fairlead}}\}^x}{\sqrt{(\{\mathbf{r}_{\text{anchor}}\}^x - \{\mathbf{r}_{\text{fairlead}}\}^x)^2 + (\{\mathbf{r}_{\text{anchor}}\}^y - \{\mathbf{r}_{\text{fairlead}}\}^y)^2}} \right]$$

The notation  $\{\mathbf{r}_{(\cdot)}\}^x / \{\mathbf{r}_{(\cdot)}\}^y$  indicates the  $x/y$  entry of the position vector  $\mathbf{r}_{(\cdot)}$ , where  $(\cdot)$  can represent the anchor or fairlead node on the  $i^{\text{th}}$  element. The linear algebraic expression in Eq. 3.2 can be reduced to the following short-hand calculation:

$$(3.5) \quad \mathbf{X}_i(s) = \mathbf{r}_i + [x_i(s) \cos \alpha_i, x_i(s) \sin \alpha_i, z_i(s)]^T$$

**3.2. Partitioned Multisegmented Solution Technique.** The solution process begins by evaluating the two continuous analytical catenary equations for each element based on  $l$  and  $h$  values obtained through node displacement relationships. An element is defined as the component connecting two adjacent nodes together. Once

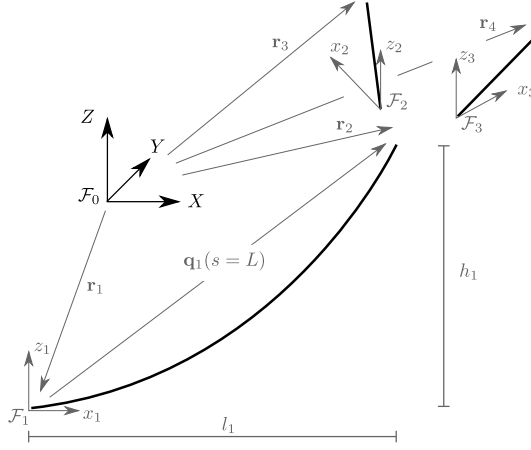


FIG. 9. Exploded representation of a 2-point bridle mooring for describing the system kinematics in assembling the multisegmented system.

the element fairlead ( $H$ ,  $V$ ) and anchor ( $H_a$ ,  $V_a$ ) values are known at the element level, the forces are transformed from the local  $x_i z_i$  frame into the global  $XYZ$  coordinate system. The force contribution at each element's anchor and fairlead is added to the corresponding node it attaches to. The force-balance equation is evaluated at the  $j^{\text{th}}$  node as follows:

$$(3.6a) \quad \{\mathbf{F}\}_X^j = \sum_{i=1}^{\text{Elements } i} [H_i \cos(\alpha_i)] - F_{X_j}^{ext} = 0$$

$$(3.6b) \quad \{\mathbf{F}\}_Y^j = \sum_{i=1}^{\text{Elements } i} [H_i \sin(\alpha_i)] - F_{Y_j}^{ext} = 0$$

$$(3.6c) \quad \{\mathbf{F}\}_Z^j = \sum_{i=1}^{\text{Elements } i} [V_i] - F_{Z_j}^{ext} + M_j g - \rho g B_j = 0$$

where  $H_i$  and  $V_i$  in the equations above correspond to  $H$  or  $H_a$  and  $V$  or  $V_a$ , depending on whether the node is a fairlead or an anchor. Based on the error of Eqs. 3.6a~3.6c, the node position is updated. As a result, the element fairlead forces must be recalculated, and the process begins again. Clearly, this process requires two distinct sets of equations, one of which must be solved within the other routine, to find the static cable configuration. The first set of equations are the force-balance relationships in three directions for each node; the second set of equations are the catenary functions. Interactions between solves is captured in the flowchart given in Figure 10. The partitioned (nested) solve procedure is summarized by the following sequence of events:

1. The problem is initialized to the extent that elements (and their properties) are defined, associations between elements and nodes are established, and user-supplied boundary conditions are declared for the model. Each node

in the array is given a classification to determine if a Newton force–balance calculation is needed.

2. An initial guess for  $\mathbf{r}_j^{(0)} = [x_j, y_j, z_j]$  is set. The guess  $\mathbf{r}_j^{(0)}$  defines initial estimates for each node (position) variable being solved.
3. Initial guesses for  $H_i^{(0)}$  and  $V_i^{(0)}$  are set.
4. The outer–loop iteration begins. The outer–loop step uses the initial state vector  $\mathbf{r}_j^{(0)}$  to iterate the element properties.
  - (a) The inner–loop iteration begins. The purpose of the inner–loop iteration is to use the continuous cable equation to solve for the unknown quantities, Eqs. 2.4a~2.4b or Eqs. 2.23a~2.23b.
  - (b) Based on the current state vector  $\mathbf{r}_j^{(0)}$  value and element initial guess  $H_i^{(0)}$  and  $V_i^{(0)}$ , the unknown components in the element state vector are solved.
  - (c) The node initial guess vector  $H_i^{(0)}$  and  $V_i^{(0)}$  is updated with  $H_i^{(1)}$  and  $V_i^{(1)}$  using a nonlinear solver.
  - (d) Once the unknowns are solved, the anchor and fairlead forces are passed to their respective attaching nodes and summed to find the total force. This concludes the inner–loop solver.
5. The force balance equation is evaluated for each non–fixed node.
6. The force balance Jacobian matrix must be evaluated using finite–difference by perturbing  $\mathbf{r}_j^{(0)} = \mathbf{r}_j^{(0)} \pm \epsilon$  and repeating steps 4(a)~4(d). This matrix is used by the outer–loop nonlinear equation solver to determine the solution for  $\mathbf{r}_j$ .
7. The node initial guess vector  $\mathbf{r}_j^{(0)}$  is updated to  $\mathbf{r}_j^{(1)}$  using an outer–loop nonlinear solver.
8. Steps 4–6 are repeated until the following objective  $\sum \mathbf{F} \leq \epsilon$  is achieved for Eqs. 3.6a~3.6c.

**3.3. Monolithic Approach.** The monolithic solution offered in this manuscript differs from the traditional nested technique in that a single–level solve is all that is needed to obtain the solution, Figure 11. This approach offers a many improvements over the conventional technique, notably:

- The solution is achieved with fewer iterations compared to the nested approach.
- The Jacobian can be computed entirely analytically.
- It enables tight coupling within the construct of the FAST modularized framework [17]

As an end result, the coupled approach leads to fewer total function evaluations since the Jacobian is computed analytically (as opposed to finite–difference, which is required with the partitioned approach). The equations being solved in the MSQS model are small in number ( $< 500$  equations typically), and iterative methods are not necessary. A direct solver is sufficient for this problem, but matrix re–ordering and change of units could be necessary for success of the approach [31, 11, 20]. However, monolithic problems can fall into pathological categories, often plagued by poor scaling

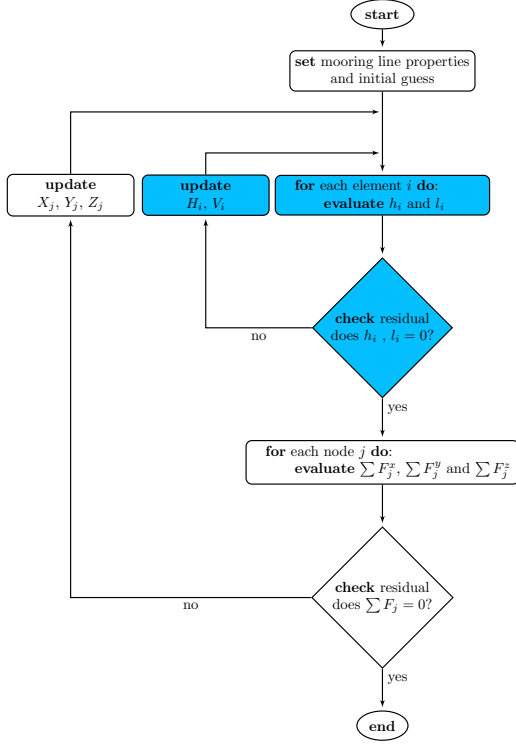


FIG. 10. *Partitioned approach to solve the MSQS problem as demonstrated in [28].*

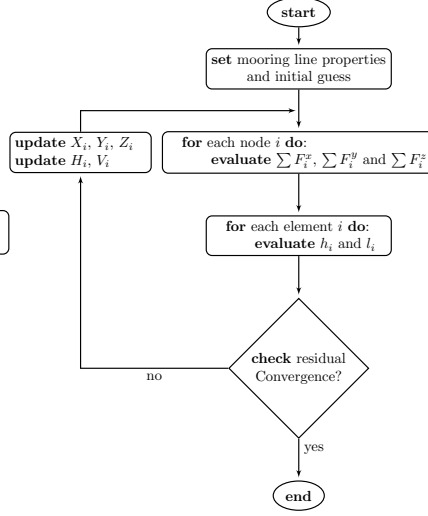


FIG. 11. *Monolithic approach to solve the MSQS problem as presented in this manuscript.*

or matrix ill-conditioning [6].

The Jacobian matrix blocks for the coupled problem can be assembled as:

$$(3.7) \quad \mathbf{J} = \begin{bmatrix} \mathbf{A} & \mathbf{B} \\ -\mathbf{B}^T & \mathbf{C} \end{bmatrix}$$

where:

- Block  $\mathbf{A} \in \mathbf{R}_{n \times n}$  are the force-balance derivatives obtained from Eqs. 3.6a~3.6c.
- Block  $\mathbf{C} \in \mathbf{R}_{m \times m}$  are the catenary equation derivatives obtained from Eqs. 2.4a~2.4b or Eqs. 2.23a~2.23b.
- Block  $\mathbf{B} \in \mathbf{R}_{n \times m}$  defines the coupled terms between  $\mathbf{A}$  and  $\mathbf{C}$ , and is dependent on the system connectivity between nodes.

This implies the Newton iteration is

$$(3.8) \quad \mathbf{z}_{N+1} = \mathbf{z}_N - \mathbf{J}^{-1} \mathbf{z}_R$$

where  $N$  refers the the Newton iteration step number, and  $\mathbf{J}$  and  $\mathbf{z}_R$  are evaluated at iteration  $N$ . Thus:

$$(3.9) \quad \mathbf{z} = [\mathbf{z}_n \ \mathbf{z}_c]^T$$

where  $\mathbf{z}_n$  are the node constraint states and  $\mathbf{z}_c$  are the catenary equation constraint states. The residual vector is the evaluation of the force-balance equations

(Eqs. 3.6a~3.6c) and the catenary equations (Eqs. 2.4a~2.4b or Eqs. 2.23a~2.23b). In the next section, the equations for the coupled MSQS solution is described. Success of this method increases with the introduction of the analytical Jacobian. The authors include an algorithm to define the Jacobian structure of the  $\mathbf{A}$  diagonal entries at run-time. Because the mooring line geometry is arbitrarily defined at run-time, the final form of the equations in  $\mathbf{A}$  and  $\mathbf{B}$  are left undefined at compile-time for flexibility. The form of the equations in  $\mathbf{A}$  is determined once at initialization, and it computed at each Newton iteration.

**4. Coupled Solution Technique.** Because the mooring system geometry is determined at run-time, the solved equations are only partially defined at compile-time. Particularly, the catenary equations (and associated Jacobian derivatives) defined by Eqs. 2.4a~2.4b or Eqs. 2.23a~2.23b are known, but the force-balance equations in Eqs. 3.6a~3.6c are assembled at run-time. Organizing the MAP program in this fashion avoids over-bearing requirements governing the definitions of an input state, model parameter, constraint, or output variable, which may restrict the scope of problems that can be solved.

To help define the process used in assembling the coupled problem, the system illustrated by Figure 4 is used as a proxy to formulate the equations and derive the Jacobian. This system contains the minimum number of distinct features to develop any generic multisegmented mooring system that could be encountered in the future, including:

1. An element resting on the seabed (Element 1).
2. A single fixed (anchor) node ( $\mathbf{r}_1$ ); this node constitutes a parameter  $\mathbf{p}$ .
3. Two fairlead nodes ( $\mathbf{r}_4$  and  $\mathbf{r}_5$ ); these nodes constitute input states  $\mathbf{u}(t)$ .
4. Two connection nodes ( $\mathbf{r}_2$  and  $\mathbf{r}_3$ ); these nodes constitute constraint states  $\mathbf{z}(t)$ .

The expanded form of the constraint states, Eq. 3.9, for this problem is:

$$(4.1a) \quad \mathbf{z}_n = [X_2 \ Y_2 \ Z_2 \ X_3 \ Y_3 \ Z_3]^T$$

and:

$$(4.1b) \quad \mathbf{z}_c = [H_1 \ V_1 \ H_2 \ V_2 \ H_3 \ V_3 \ H_4 \ V_4]^T$$

The residuals,  $\mathbf{Z}_R$ , are the functions solved by the root-finder. The equations solved for the connecting nodes are the force-balance equations, specifically:

$$(4.2) \quad \mathbf{Z}_{R_n} = \begin{bmatrix} F_{x_2} \\ F_{y_2} \\ F_{z_2} \\ F_{x_3} \\ F_{y_3} \\ F_{z_3} \end{bmatrix} = \begin{bmatrix} H_{F_1} \cos \alpha_1 + H_{A_2} \cos \alpha_2 \\ H_{F_1} \sin \alpha_1 + H_{A_2} \sin \alpha_2 \\ V_{F_1} + V_{A_2} \\ H_{F_2} \cos \alpha_2 + H_{A_3} \cos \alpha_3 + H_{A_4} \cos \alpha_4 \\ H_{F_2} \sin \alpha_2 + H_{A_3} \sin \alpha_3 + H_{A_4} \sin \alpha_4 \\ V_{F_2} + V_{A_3} + V_{A_4} \end{bmatrix}$$

The expressions  $\cos \alpha_i$  and  $\sin \alpha_i$  are shorthand for:

$$(4.3a) \quad \cos \alpha_i = \frac{X_{f_i} - X_{a_i}}{\sqrt{(X_{f_i} - X_{a_i})^2 + (Y_{f_i} - Y_{a_i})^2}}$$

$$(4.3b) \quad \sin \alpha_i = \frac{Y_{f_i} - Y_{a_i}}{\sqrt{(X_{f_i} - X_{a_i})^2 + (Y_{f_i} - Y_{a_i})^2}}$$

which are the necessary forms to derive the analytical Jacobian. For clarification, the nodes in Figure 4 are labeled from 1~5, whereas, Eqs. 4.3a~4.3b is paired with two nodes since an element requires one fairlead and one anchor point. Nodes between elements can be shared, and under this definition, the following can be surmised for node 2:

$$(4.4a) \quad X_2 = \{\mathbf{r}_{f_1}\}_X = \{\mathbf{r}_{a_2}\}_X$$

$$(4.4b) \quad X_3 = \{\mathbf{r}_{f_2}\}_X = \{\mathbf{r}_{a_3}\}_X = \{\mathbf{r}_{a_4}\}_X$$

The residual function for the closed-form catenary equations appear as:

$$(4.5) \quad \mathbf{Z}_{R_c} = [l_1 \ h_1 \ l_2 \ h_2 \ l_3 \ h_3 \ l_4 \ h_5]^T$$

Equations 4.2 and 4.5 combine to construct the residual:

$$(4.6) \quad \mathbf{Z}_R = [\mathbf{Z}_{R_n} \ \mathbf{Z}_{R_c}]^T$$

Based on the structure of Eq. 4.6 and the matrix block notion in Eq. 3.7, the Jacobian matrix for the problem illustrated in Figure 4 can be formulated as:

$$(4.7) \quad \mathbf{J} = \begin{bmatrix} \frac{\partial\{F_{x2}\}}{\partial X_2} & \frac{\partial\{F_{x2}\}}{\partial Y_2} & \frac{\partial\{F_{x2}\}}{\partial Z_2} & \frac{\partial\{F_{x2}\}}{\partial X_3} & \frac{\partial\{F_{x2}\}}{\partial Y_3} & \frac{\partial\{F_{x2}\}}{\partial Z_3} & \frac{\partial\{F_{x2}\}}{\partial H_1} & \frac{\partial\{F_{x2}\}}{\partial V_1} & \frac{\partial\{F_{x2}\}}{\partial H_2} & \frac{\partial\{F_{x2}\}}{\partial V_2} & \frac{\partial\{F_{x2}\}}{\partial H_3} & \frac{\partial\{F_{x2}\}}{\partial V_3} & \frac{\partial\{F_{x2}\}}{\partial H_4} & \frac{\partial\{F_{x2}\}}{\partial V_4} \\ \frac{\partial\{F_{y2}\}}{\partial X_2} & \frac{\partial\{F_{y2}\}}{\partial Y_2} & \frac{\partial\{F_{y2}\}}{\partial Z_2} & \frac{\partial\{F_{y2}\}}{\partial X_3} & \frac{\partial\{F_{y2}\}}{\partial Y_3} & \frac{\partial\{F_{y2}\}}{\partial Z_3} & \frac{\partial\{F_{y2}\}}{\partial H_1} & \frac{\partial\{F_{y2}\}}{\partial V_1} & \frac{\partial\{F_{y2}\}}{\partial H_2} & \frac{\partial\{F_{y2}\}}{\partial V_2} & \frac{\partial\{F_{y2}\}}{\partial H_3} & \frac{\partial\{F_{y2}\}}{\partial V_3} & \frac{\partial\{F_{y2}\}}{\partial H_4} & \frac{\partial\{F_{y2}\}}{\partial V_4} \\ \frac{\partial\{F_{z2}\}}{\partial X_2} & \frac{\partial\{F_{z2}\}}{\partial Y_2} & \frac{\partial\{F_{z2}\}}{\partial Z_2} & \frac{\partial\{F_{z2}\}}{\partial X_3} & \frac{\partial\{F_{z2}\}}{\partial Y_3} & \frac{\partial\{F_{z2}\}}{\partial Z_3} & \frac{\partial\{F_{z2}\}}{\partial H_1} & \frac{\partial\{F_{z2}\}}{\partial V_1} & \frac{\partial\{F_{z2}\}}{\partial H_2} & \frac{\partial\{F_{z2}\}}{\partial V_2} & \frac{\partial\{F_{z2}\}}{\partial H_3} & \frac{\partial\{F_{z2}\}}{\partial V_3} & \frac{\partial\{F_{z2}\}}{\partial H_4} & \frac{\partial\{F_{z2}\}}{\partial V_4} \\ \frac{\partial\{F_{x3}\}}{\partial X_2} & \frac{\partial\{F_{x3}\}}{\partial Y_2} & \frac{\partial\{F_{x3}\}}{\partial Z_2} & \frac{\partial\{F_{x3}\}}{\partial X_3} & \frac{\partial\{F_{x3}\}}{\partial Y_3} & \frac{\partial\{F_{x3}\}}{\partial Z_3} & \frac{\partial\{F_{x3}\}}{\partial H_1} & \frac{\partial\{F_{x3}\}}{\partial V_1} & \frac{\partial\{F_{x3}\}}{\partial H_2} & \frac{\partial\{F_{x3}\}}{\partial V_2} & \frac{\partial\{F_{x3}\}}{\partial H_3} & \frac{\partial\{F_{x3}\}}{\partial V_3} & \frac{\partial\{F_{x3}\}}{\partial H_4} & \frac{\partial\{F_{x3}\}}{\partial V_4} \\ \frac{\partial\{F_{y3}\}}{\partial X_2} & \frac{\partial\{F_{y3}\}}{\partial Y_2} & \frac{\partial\{F_{y3}\}}{\partial Z_2} & \frac{\partial\{F_{y3}\}}{\partial X_3} & \frac{\partial\{F_{y3}\}}{\partial Y_3} & \frac{\partial\{F_{y3}\}}{\partial Z_3} & \frac{\partial\{F_{y3}\}}{\partial H_1} & \frac{\partial\{F_{y3}\}}{\partial V_1} & \frac{\partial\{F_{y3}\}}{\partial H_2} & \frac{\partial\{F_{y3}\}}{\partial V_2} & \frac{\partial\{F_{y3}\}}{\partial H_3} & \frac{\partial\{F_{y3}\}}{\partial V_3} & \frac{\partial\{F_{y3}\}}{\partial H_4} & \frac{\partial\{F_{y3}\}}{\partial V_4} \\ \frac{\partial\{F_{z3}\}}{\partial X_2} & \frac{\partial\{F_{z3}\}}{\partial Y_2} & \frac{\partial\{F_{z3}\}}{\partial Z_2} & \frac{\partial\{F_{z3}\}}{\partial X_3} & \frac{\partial\{F_{z3}\}}{\partial Y_3} & \frac{\partial\{F_{z3}\}}{\partial Z_3} & \frac{\partial\{F_{z3}\}}{\partial H_1} & \frac{\partial\{F_{z3}\}}{\partial V_1} & \frac{\partial\{F_{z3}\}}{\partial H_2} & \frac{\partial\{F_{z3}\}}{\partial V_2} & \frac{\partial\{F_{z3}\}}{\partial H_3} & \frac{\partial\{F_{z3}\}}{\partial V_3} & \frac{\partial\{F_{z3}\}}{\partial H_4} & \frac{\partial\{F_{z3}\}}{\partial V_4} \\ \frac{\partial l_1}{\partial X_2} & \frac{\partial l_1}{\partial Y_2} & \frac{\partial l_1}{\partial Z_2} & \frac{\partial l_1}{\partial X_3} & \frac{\partial l_1}{\partial Y_3} & \frac{\partial l_1}{\partial Z_3} & \frac{\partial l_1}{\partial H_1} & \frac{\partial l_1}{\partial V_1} & \frac{\partial l_1}{\partial H_2} & \frac{\partial l_1}{\partial V_2} & \frac{\partial l_1}{\partial H_3} & \frac{\partial l_1}{\partial V_3} & \frac{\partial l_1}{\partial H_4} & \frac{\partial l_1}{\partial V_4} \\ \frac{\partial h_1}{\partial X_2} & \frac{\partial h_1}{\partial Y_2} & \frac{\partial h_1}{\partial Z_2} & \frac{\partial h_1}{\partial X_3} & \frac{\partial h_1}{\partial Y_3} & \frac{\partial h_1}{\partial Z_3} & \frac{\partial h_1}{\partial H_1} & \frac{\partial h_1}{\partial V_1} & \frac{\partial h_1}{\partial H_2} & \frac{\partial h_1}{\partial V_2} & \frac{\partial h_1}{\partial H_3} & \frac{\partial h_1}{\partial V_3} & \frac{\partial h_1}{\partial H_4} & \frac{\partial h_1}{\partial V_4} \\ \frac{\partial l_2}{\partial X_2} & \frac{\partial l_2}{\partial Y_2} & \frac{\partial l_2}{\partial Z_2} & \frac{\partial l_2}{\partial X_3} & \frac{\partial l_2}{\partial Y_3} & \frac{\partial l_2}{\partial Z_3} & \frac{\partial l_2}{\partial H_1} & \frac{\partial l_2}{\partial V_1} & \frac{\partial l_2}{\partial H_2} & \frac{\partial l_2}{\partial V_2} & \frac{\partial l_2}{\partial H_3} & \frac{\partial l_2}{\partial V_3} & \frac{\partial l_2}{\partial H_4} & \frac{\partial l_2}{\partial V_4} \\ \frac{\partial h_2}{\partial X_2} & \frac{\partial h_2}{\partial Y_2} & \frac{\partial h_2}{\partial Z_2} & \frac{\partial h_2}{\partial X_3} & \frac{\partial h_2}{\partial Y_3} & \frac{\partial h_2}{\partial Z_3} & \frac{\partial h_2}{\partial H_1} & \frac{\partial h_2}{\partial V_1} & \frac{\partial h_2}{\partial H_2} & \frac{\partial h_2}{\partial V_2} & \frac{\partial h_2}{\partial H_3} & \frac{\partial h_2}{\partial V_3} & \frac{\partial h_2}{\partial H_4} & \frac{\partial h_2}{\partial V_4} \\ \frac{\partial l_3}{\partial X_2} & \frac{\partial l_3}{\partial Y_2} & \frac{\partial l_3}{\partial Z_2} & \frac{\partial l_3}{\partial X_3} & \frac{\partial l_3}{\partial Y_3} & \frac{\partial l_3}{\partial Z_3} & \frac{\partial l_3}{\partial H_1} & \frac{\partial l_3}{\partial V_1} & \frac{\partial l_3}{\partial H_2} & \frac{\partial l_3}{\partial V_2} & \frac{\partial l_3}{\partial H_3} & \frac{\partial l_3}{\partial V_3} & \frac{\partial l_3}{\partial H_4} & \frac{\partial l_3}{\partial V_4} \\ \frac{\partial h_3}{\partial X_2} & \frac{\partial h_3}{\partial Y_2} & \frac{\partial h_3}{\partial Z_2} & \frac{\partial h_3}{\partial X_3} & \frac{\partial h_3}{\partial Y_3} & \frac{\partial h_3}{\partial Z_3} & \frac{\partial h_3}{\partial H_1} & \frac{\partial h_3}{\partial V_1} & \frac{\partial h_3}{\partial H_2} & \frac{\partial h_3}{\partial V_2} & \frac{\partial h_3}{\partial H_3} & \frac{\partial h_3}{\partial V_3} & \frac{\partial h_3}{\partial H_4} & \frac{\partial h_3}{\partial V_4} \\ \frac{\partial l_4}{\partial X_2} & \frac{\partial l_4}{\partial Y_2} & \frac{\partial l_4}{\partial Z_2} & \frac{\partial l_4}{\partial X_3} & \frac{\partial l_4}{\partial Y_3} & \frac{\partial l_4}{\partial Z_3} & \frac{\partial l_4}{\partial H_1} & \frac{\partial l_4}{\partial V_1} & \frac{\partial l_4}{\partial H_2} & \frac{\partial l_4}{\partial V_2} & \frac{\partial l_4}{\partial H_3} & \frac{\partial l_4}{\partial V_3} & \frac{\partial l_4}{\partial H_4} & \frac{\partial l_4}{\partial V_4} \\ \frac{\partial h_4}{\partial X_2} & \frac{\partial h_4}{\partial Y_2} & \frac{\partial h_4}{\partial Z_2} & \frac{\partial h_4}{\partial X_3} & \frac{\partial h_4}{\partial Y_3} & \frac{\partial h_4}{\partial Z_3} & \frac{\partial h_4}{\partial H_1} & \frac{\partial h_4}{\partial V_1} & \frac{\partial h_4}{\partial H_2} & \frac{\partial h_4}{\partial V_2} & \frac{\partial h_4}{\partial H_3} & \frac{\partial h_4}{\partial V_3} & \frac{\partial h_4}{\partial H_4} & \frac{\partial h_4}{\partial V_4} \\ \frac{\partial l_5}{\partial X_2} & \frac{\partial l_5}{\partial Y_2} & \frac{\partial l_5}{\partial Z_2} & \frac{\partial l_5}{\partial X_3} & \frac{\partial l_5}{\partial Y_3} & \frac{\partial l_5}{\partial Z_3} & \frac{\partial l_5}{\partial H_1} & \frac{\partial l_5}{\partial V_1} & \frac{\partial l_5}{\partial H_2} & \frac{\partial l_5}{\partial V_2} & \frac{\partial l_5}{\partial H_3} & \frac{\partial l_5}{\partial V_3} & \frac{\partial l_5}{\partial H_4} & \frac{\partial l_5}{\partial V_4} \\ \frac{\partial h_5}{\partial X_2} & \frac{\partial h_5}{\partial Y_2} & \frac{\partial h_5}{\partial Z_2} & \frac{\partial h_5}{\partial X_3} & \frac{\partial h_5}{\partial Y_3} & \frac{\partial h_5}{\partial Z_3} & \frac{\partial h_5}{\partial H_1} & \frac{\partial h_5}{\partial V_1} & \frac{\partial h_5}{\partial H_2} & \frac{\partial h_5}{\partial V_2} & \frac{\partial h_5}{\partial H_3} & \frac{\partial h_5}{\partial V_3} & \frac{\partial h_5}{\partial H_4} & \frac{\partial h_5}{\partial V_4} \end{bmatrix}$$

where  $x_i$ ,  $y_i$ , and  $z_i$  can function as either a fairlead or an anchor for a particular node. The matrix in Eq. 4.7 is divided into **A**, **B**, and **C** blocks based on the pattern in Eq. 3.7. Different colors within sub-blocks identify the cells where different algorithms are employed to calculate the derivatives. The unshaded entries are zero-valued. In total, five different algorithms are necessary. As noted earlier, the structure for the **C** matrix block is decided at compile-time, but **A** and **B** both depend on the system geometry, which is determined at run-time. The next section highlights the technique employed in MAP to determine the equations for all three blocks.

**4.1. A-Block Derivatives.** Allowing  $H_X = H \cos \alpha$ , Eq. 4.2 can be differentiated to show:

$$(4.8a) \quad \frac{\partial H_X}{\partial X_f} = H \frac{(Y_f - Y_a)^2}{\left[ (X_f - X_a)^2 + (Y_f - Y_a)^2 \right]^{3/2}}$$

$$(4.8b) \quad \frac{\partial H_X}{\partial X_a} = -\frac{\partial H_X}{\partial X_f}$$

$$(4.8c) \quad \frac{\partial H_X}{\partial Y_f} = -H \frac{(X_f - X_a)(Y_f - Y_a)}{\left[(X_f - X_a)^2 + (Y_f - Y_a)^2\right]^{3/2}}$$

$$(4.8d) \quad \frac{\partial H_X}{\partial Y_a} = -\frac{\partial H_X}{\partial Y_f}$$

Likewise,  $H_Y = H \sin \alpha$  can be shown to be:

$$(4.9a) \quad \frac{\partial H_Y}{\partial X_f} = -H \frac{(X_f - X_a)(Y_f - Y_a)}{\left[(X_f - X_a)^2 + (Y_f - Y_a)^2\right]^{3/2}}$$

$$(4.9b) \quad \frac{\partial H_Y}{\partial X_a} = -\frac{\partial H_Y}{\partial X_f}$$

$$(4.9c) \quad \frac{\partial H_Y}{\partial Y_f} = H \frac{(X_f - X_a)^2}{\left[(X_f - X_a)^2 + (Y_f - Y_a)^2\right]^{3/2}}$$

$$(4.9d) \quad \frac{\partial H_Y}{\partial Y_a} = -\frac{\partial H_Y}{\partial Y_f}$$

**4.1.1. Diagonal Components.** Eqs. 4.9~4.10 represent the derivatives for a single line element. In the case of a multisegmented system, the derivative along the diagonal  $\mathbf{A}$  block is a summation of these terms. For example, taking the derivative of the first term in Eq. 4.2 leads to:

$$(4.10a) \quad \frac{\partial (H_{F_1} \cos \alpha_1 + H_{A_2} \cos \alpha_2)}{\partial X_2} = H_{F_1} \frac{(Y_2 - Y_1)^2}{\left[(X_2 - X_1)^2 + (Y_2 - Y_1)^2\right]^{3/2}} \left. \vphantom{\frac{\partial (H_{F_1} \cos \alpha_1 + H_{A_2} \cos \alpha_2)}{\partial X_2}} \right\} \text{Element 1}$$

$$+ H_{A_2} \frac{(Y_3 - Y_2)^2}{\left[(X_3 - X_2)^2 + (Y_3 - Y_2)^2\right]^{3/2}} \left. \vphantom{\frac{\partial (H_{F_1} \cos \alpha_1 + H_{A_2} \cos \alpha_2)}{\partial X_2}} \right\} \text{Element 2}$$

Note that node 2 constitutes the fairlead of element 1 and anchor of element 2. Likewise, taking the derivative with respect to  $Y_2$  leads to:

$$(4.10b) \quad \frac{\partial (H_{F_1} \cos \alpha_1 + H_{A_2} \cos \alpha_2)}{\partial Y_2} = H_{F_1} \frac{(X_2 - X_1)(Y_2 - Y_1)}{\left[(X_2 - X_1)^2 + (Y_2 - Y_1)^2\right]^{3/2}} \left. \vphantom{\frac{\partial (H_{F_1} \cos \alpha_1 + H_{A_2} \cos \alpha_2)}{\partial Y_2}} \right\} \text{Element 1}$$

$$+ H_{A_2} \frac{(X_3 - X_2)(Y_3 - Y_2)}{\left[(X_3 - X_2)^2 + (Y_3 - Y_2)^2\right]^{3/2}} \left. \vphantom{\frac{\partial (H_{F_1} \cos \alpha_1 + H_{A_2} \cos \alpha_2)}{\partial Y_2}} \right\} \text{Element 2}$$

It is apparent the derivatives along the diagonal of block  $\mathbf{A}$  in Eq. 4.7 are a summation of derivatives. This observation is taken advantage of in MAP to allow the Jacobian to be formulated as the kinematic chain of elements are assembled during model initialization. The computation in Eqs. 4.10a~4.10b is executed at each Newton iteration step using the following command:

```

for  $i = 1$  : number of non-zero entries in A do
     $row = JacA[i].row$ 
     $col = JacA[i].col$ 
     $\mathbf{A}[row][col] \leftarrow JacA[i].get\_derivative()$ 
end

```

where  $JacA$  is a class (object) containing all the individual derivative components in Eqs. 41~42. The algorithm above is contrived for simpler conveyance of principles, but  $JacA$  is a vector whose size equals the number of non-zero entries in the  $\mathbf{A}$  matrix block, and is assembled using Algorithm 1 at model initialization. The expensive component of the computation is assembling and defining equations in  $\mathbf{A}$ , which is only performed once. The off-diagonal components of  $\mathbf{A}$  are assembled in a similar fashion, allowing the Jacobian to be computed efficiently.

**4.2. B-Block Derivatives.** Matrix  $\mathbf{B}$  is the term coupling  $\mathbf{A}$  and  $\mathbf{C}$  together, and its structure depends on the system connectivity geometry. The  $\mathbf{B}$  block in Eq. 3.7 is assembled by differentiating Eq. 4.2 with respect to the constraint variables  $H_i$  and  $V_i$ . Equation 2.3a also illustrates  $H_a = H$ , revealing the derivatives reduce to  $\cos \alpha_i$  or  $\sin \alpha_i$  terms.

$$(4.11) \quad \mathbf{B}_i = \begin{bmatrix} \cos \alpha_i & 0 \\ \sin \alpha_i & 0 \\ 0 & 1 \end{bmatrix}$$

The composition of Jacobian block  $\mathbf{B}$  is assembled using:

$$(4.12) \quad \mathbf{B} = \begin{bmatrix} \mathbf{B}_1 & \mathbf{B}_2 & 0 & 0 \\ 0 & \mathbf{B}_2 & \mathbf{B}_3 & \mathbf{B}_4 \end{bmatrix}$$

The number of rows in  $\mathbf{B}$  is equal to the number of nodes being iterated in the system, and each row accounts for the elements attaching to the node in question. In the example of row 2 in  $\mathbf{B}$ , elements 2, 3, and 4 attach to node 3, so the element is populated with  $\mathbf{B}_2$ ,  $\mathbf{B}_3$ , and  $\mathbf{B}_4$  entries. The structure in Eq. 4.12 is specific to the geometry given by the system in Figure 4, but the structure of other generic systems can be inferred by it.

**4.3. C-Block Derivatives.** The  $\mathbf{C}$  matrix block is composed entirely of derivatives using the close-form catenary equations, either Eqs. 2.4a~2.4b for the case of a hanging chain or Eqs. 2.23a~2.23b if the cable is resting on the seabed. The composition of the  $\mathbf{C}$  block is:

$$(4.13) \quad \mathbf{C}_i = \begin{bmatrix} \frac{\partial l_i}{\partial H_i} & \frac{\partial l_i}{\partial V_i} \\ \frac{\partial h_i}{\partial H_i} & \frac{\partial h_i}{\partial V_i} \end{bmatrix}$$

with:

$$(4.14) \quad \mathbf{C} = \begin{bmatrix} \mathbf{C}_1 & 0 & 0 \\ 0 & \ddots & 0 \\ 0 & 0 & \mathbf{C}_M \end{bmatrix}$$

```

1 begin
2   initialize row = 0
3   for i = 1 : length node do
4     row += 1
5     A_cell = new Jacobian entry in A block
6     for j = 1 : length element do
7       if (node[i] ∈ element[j].fairlead) then
8         deriv = null
9         switch direction {X,Y} being iterated do
10          case X
11            deriv ← ∂HX / ∂Xf (element[j])
12          case Y
13            deriv ← ∂HY / ∂Xf (element[j])
14          end
15          A_cell += deriv
16        if (node[i] ∈ element[j].anchor) then
17          deriv = null
18          switch direction {X,Y} being iterated do
19            case X
20              deriv ← ∂HX / ∂Xa (element[j])
21            case Y
22              deriv ← ∂HY / ∂Xa (element[j])
23            end
24            A_cell += deriv
25          end
26          JacA.push_back ( A_cell )
27          N = size JacA
28          JacA[N].row = row
29          JacA[N].col = row
30        end
31      end

```

**Algorithm 1:** Process illustrating the assembly of the diagonal components in the **A** matrix.

The individual components of Eq. 4.13 have to be derived, which are done so in the following two subsections.

**4.3.1. Hanging Chain.** The equation satisfying a hanging chain applies when Eq. 2.6 is satisfied. In this scenario, the derivatives for Eq. 4.13 are:

$$(4.15a) \quad \frac{\partial l}{\partial H} = \frac{1}{\omega} \left\{ \ln \left[ \frac{V}{H} + \sqrt{1 + \left( \frac{V}{H} \right)^2} \right] - \ln \left[ \frac{V - \omega L}{H} + \sqrt{1 + \left( \frac{V - \omega L}{H} \right)^2} \right] \right\} \\
- \frac{1}{\omega} \left\{ \frac{\frac{V}{H} + \frac{\left(\frac{V}{H}\right)^2}{\sqrt{1 + \left(\frac{V}{H}\right)^2}}}{\frac{V}{H} + \sqrt{1 + \left(\frac{V}{H}\right)^2}} - \frac{\frac{V - \omega L}{H} + \frac{\left(\frac{V - \omega L}{H}\right)^2}{\sqrt{1 + \left(\frac{V - \omega L}{H}\right)^2}}}{\frac{V - \omega L}{H} + \sqrt{1 + \left(\frac{V - \omega L}{H}\right)^2}} \right\} + \frac{L}{EA}$$

$$(4.15b) \quad \frac{\partial l}{\partial V} = \frac{1}{\omega} \left[ \frac{1 + \frac{V}{H\sqrt{1+(\frac{V}{H})^2}}}{\frac{V}{H} + \sqrt{1+(\frac{V}{H})^2}} - \frac{1 + \frac{V-\omega L}{H\sqrt{1+(\frac{V-\omega L}{H})^2}}}{\frac{V-\omega L}{H} + \sqrt{1+(\frac{V-\omega L}{H})^2}} \right]$$

$$(4.15c) \quad \frac{\partial h}{\partial H} = \frac{1}{\omega} \left[ \sqrt{1 + \left(\frac{V}{H}\right)^2} - \sqrt{1 + \left(\frac{V-\omega L}{H}\right)^2} \right] \\ - \frac{1}{\omega} \left[ \frac{V^2}{H^2\sqrt{1+(\frac{V}{H})^2}} - \frac{(V-\omega L)^2}{H^2\sqrt{1+(\frac{V-\omega L}{H})^2}} \right]$$

$$(4.15d) \quad \frac{\partial h}{\partial V} = \frac{1}{\omega} \left[ \frac{V}{H\sqrt{1+(\frac{V}{H})^2}} - \frac{V-\omega L}{H\sqrt{1+(\frac{V-\omega L}{H})^2}} \right] + \frac{L}{EA}$$

**4.3.2. Cable in Contact with Seabed.** For the case of a cable in contact with the seabed, the governing derivatives apply depending on whether the anchor force is greater than zero. When  $H_a \leq 0$ , the equation satisfying Eq. 4.13 are:

$$(4.16a) \quad \frac{\partial l}{\partial V} = \frac{C_B}{EA} \left( L - \frac{V}{\omega} \right) + \frac{1}{\omega} \left[ \frac{1 + \frac{V}{H\sqrt{1+(\frac{V}{H})^2}}}{\frac{V}{H} + \sqrt{1+(\frac{V}{H})^2}} - 1 \right]$$

$$(4.16b) \quad \frac{\partial h}{\partial H} = \frac{1}{\omega} \left[ \sqrt{1 + \left(\frac{V}{H}\right)^2} - 1 \right] - \frac{1}{\omega} \left[ \frac{V^2}{H^2\sqrt{1+(\frac{V}{H})^2}} \right]$$

$$(4.16c) \quad \frac{\partial h}{\partial V} = \frac{1}{\omega} \left[ \frac{V}{H\sqrt{1+(\frac{V}{H})^2}} \right] + \frac{V}{\omega EA}$$

The final derivative for  $\frac{\partial l}{\partial H}$  is conditional depending on whether  $H_a > 0$ .

$$(4.16d) \quad \frac{\partial l}{\partial H} = \begin{cases} \frac{L}{EA} + \frac{1}{\omega} \ln \left[ \frac{V}{H} + \sqrt{1 + \left(\frac{V}{H}\right)^2} \right] - \frac{1}{\omega} \left[ \frac{\frac{V}{H} + \frac{V^2}{H^2\sqrt{1+(\frac{V}{H})^2}}}{\frac{V}{H} + \sqrt{1+(\frac{V}{H})^2}} \right] & \text{if } x_0 \leq 0 \\ \frac{L}{EA} - \frac{1}{EA} \left( L - \frac{V}{\omega} - \frac{H}{C_B\omega} \right) + \frac{1}{\omega} \ln \left[ \frac{V}{H} + \sqrt{1 + \left(\frac{V}{H}\right)^2} \right] - \frac{1}{\omega} \left[ \frac{\frac{V}{H} + \frac{V^2}{H^2\sqrt{1+(\frac{V}{H})^2}}}{\frac{V}{H} + \sqrt{1+(\frac{V}{H})^2}} \right] & \text{if } x_0 > 0 \end{cases}$$

**5. Example.** Five different strategies to solve the problem pictured in Figure 12 are carried out using different algorithms using both the partitioned and monolithic strategies outlined in this paper. The purpose of this exercise is to demonstrate the performance of the coupled multi-physics approach presented in this manuscript against the nested iterative technique shown in Figure 10. This hypothetical problem depicts a two line mooring system deployed at a water depth of 350 meters. The anchor points are fixed, and the fairlead intersect at a common point. A buoyancy module is attached at the intersection of fairleads, and it produces a reaction force of  $F_z = 637.65$  kN. The mooring lines are composed of synthetic material, with the full properties of the two mooring lines:

- $EA = 2.34 \times 10^5$  kN
- $\omega = 226.61$  N/m
- $L_1 = 1175$  m
- $L_2 = 300$  m
- $\mathbf{r}_{a_1} = [-1200, 0, -350]$  m
- $\mathbf{r}_{a_2} = [0, 0, -350]$  m

The user-supplied initial guesses in all examples are given as:

$$(5.1) \quad \mathbf{z}_c = \begin{bmatrix} H_1^{(0)} & V_1^{(0)} & H_2^{(0)} & V_2^{(0)} \end{bmatrix}^T = [168.7 \ 752.7 \ 1.4 \ 168.1]^T \text{ kN}$$

for the line fairlead forces, and for the node displacements:

$$(5.2) \quad \mathbf{z}_n = \begin{bmatrix} X_2^{(0)} & Y_2^{(0)} & Z_2^{(0)} \end{bmatrix}^T = [-26.0 \ 0.0 \ -65.0]^T \text{ m}$$

In Table 2, the performance of partitioned solution approach is compared to four different numerical implementations of the monolithic approach. A Levenberg–Marquardt non-linear solver was used for the partitioned approach [24]. Although a different numerical algorithm was used in [28], the Levenberg–Marquardt provides robustness to solve problems with arbitrary line types and configurations without needing to manually relaxed the Newton iteration step size to prevent overshoot of the solution. In the example in Figure 12, the solution is achieved with 90 inner-loop iterations and 24 outer-loop iterations (In this context, inner-loop iterations occur when the catenary equations are evaluated, and outer-loop iterations take place when the force-balance equations are evaluated). The number of function evaluations does not include entries for calculating the Jacobian through finite difference, as the intention of this exercise is to measure the number of Newton iteration steps from initial guess to solution. As a result, the frequency of function evaluations during the Jacobian calculation would depend on the finite-difference stencil (i.e., centered finite-difference versus forward finite-difference).

The monolithic MSQS strategy was implemented with various solver options to 1) test performance of the technique using the analytically-derived Jacobian and 2) test performance against different non-linear solvers. To improve matrix conditioning, the units for the force variables were modified from [N] to [kN]. This not also affects the residual function  $\mathbf{Z}_{R_n}$  in Eq. 4.2, but also the  $\mathbf{A}$  and  $\mathbf{B}$  matrix block in Eq. 3.7 (but not the  $-\mathbf{B}^T$  matrix block). The two non-linear solvers utilized are a Newton line-search method and a trust region method [26]. Upon inspection of the various methods, we find that invoking the analytical Jacobian results in marginally greater accuracy, while the the total number of iterations for the coupled problems

results in far fewer compared to the nested approach: nearly an order of magnitude of two. Differences between the analytical and numerically-computed Jacobian were also compared to determine if errors exist in the Jacobian calculation. The ‘norm difference’ is calculated using:

$$(5.3) \quad \text{norm difference} = \|\mathbf{J}_{fd} - \mathbf{J}_{analytical}\|$$

where the Jacobians are evaluated at the user-defined initial guess. The norm difference of this problem was calculated to be  $6.18 \times 10^{-6}$ . At convergence, the final solution of the system pictured in Figure 12 is:

$$(5.4) \quad \mathbf{z}_c = \left[ H_1^{(f)} \ V_1^{(f)} \ H_2^{(f)} \ V_2^{(f)} \right]^T = [137.8 \ 566.6 \ 137.8 \ 71.1]^T \text{ kN}$$

for the fairlead forces and:

$$(5.5) \quad \mathbf{z}_n = \left[ X_2^{(f)} \ Y_2^{(f)} \ Z_2^{(f)} \right]^T = [-72.1 \ 0.0 \ -58.0]^T \text{ m}$$

Note that  $H_1 = H_2$ , which is a requirement for static equilibrium per Eqs. 30. Identical solutions are achieved using either the partitioned or monolithic approaches.

The computational cost of evaluating the inverse of a Jacobian is proportional to the cube of the matrix dimension  $n$ :

$$(5.6) \quad \mathbf{J}_{n \times n}^{-1} = \mathcal{O}\left(\frac{2}{3}n^3\right)$$

This in turn relates the amount of computational resources needed at each iteration of the solve. Because matrix inversion is proportional to  $n^3$ , direct solvers are avoided for large matrices. One advantage of the partitioned solver is that it requires the inversion of two smaller matrices, whereas the monolithic algorithm requires the inversion of one larger matrix. Once a problem reaches a certain size, the computational resources for the monolithic algorithm may exceed the partitioned approach. Table 2 records the number of multiplication operations needed for matrix inversion using LU factorization. This is calculated based on total number of iterations, Jacobian size, and Eq. 5.6. For example, for the monolithic approach:

$$(5.7) \quad \mathbf{J}_{7 \times 7}^{-1} \text{ operations} = 7 \times \frac{2}{3} \times 7^3 = 1,600$$

In this example, the matrix inversion is 2.67 times more rigorous for the partitioned (nested) approach compared to the monolithic approach. An advantage not being exploited in the partitioned algorithm is the manner in which the inverse Jacobian evaluation is performed. The partitioned algorithm retains the identical pattern of Eq. 4.14, which is a diagonal arrangement of sequential  $2 \times 2$  block matrices. Inverting this matrix is done trivially user Cramer’s rule. Invoking this strategy and using the analytical Jacobian published in this manuscript would be an improvement of the method illustrated by [28], thus lowering the computational expense by significant margins.

**6. Summary and Conclusion.** A new method to calculate the solution to a multisegmented, quasi-static cable system is presented in this manuscript. Through analysis of an example, the monolithic algorithm was developed and demonstrated

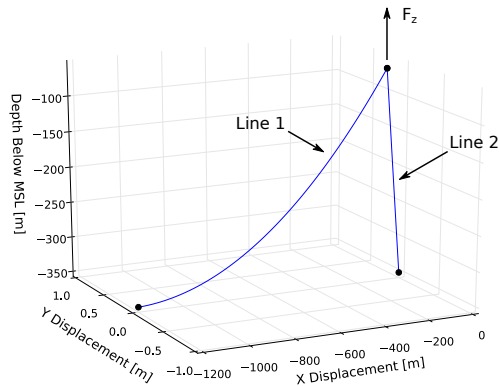


FIG. 12. Example used to demonstrate performance of the coupled multi-physics approach in MAP's MSQS module against the nested solution techniques.

TABLE 2

Number of iterations required to achieve the solution for the multi-segmented system in Figure 12. The function norm  $\|\mathbf{Z}_R\|$  is the magnitude of the residual at the final iteration. The number of multiplication operations to calculate the inverse of  $\mathbf{J}$  based on Eq. 5.6. The step size and function evaluation tolerances are set to  $1 \times 10^{-6}$  for all nonlinear solvers.

	$\ \mathbf{Z}_R\ $	Function Evaluations	Total $\mathbf{J}^{-1}$ Multiplication Operations
<b>Nested</b> Levenberg-Marquardt	$\ \mathbf{Z}_n\  = 0.18$ $\ \mathbf{Z}_n\  = 2.74 \times 10^{-7}$	Outer Loop: 24 Inner Loop: 90	4,272
<b>MSQS</b> fd Jacobian trust region	$2.04 \times 10^{-5}$	7	1,600
<b>MSQS</b> analytical Jacobian trust region	$2.04 \times 10^{-5}$	7	1,600
<b>MSQS</b> fd Jacobian line search	$2.08 \times 10^{-9}$	7	1,600
<b>MSQS</b> analytical Jacobian line search	$2.10 \times 10^{-9}$	7	1,600

to require fewer non-linear solve iterations to achieve convergence compared to traditional nested (partitioned) techniques. To improve computational efficiency and accuracy, a process for computing the Jacobian analytically was also specified. The use of an analytical Jacobian can improve efficiency, and benefits of the analytically-obtained Jacobian become more apparent as the problem size grows (since finite-differencing methods require more function evaluations). The use of the analytical

Jacobian is recommended because finite-difference is sensitive to machine precision, and the level of accuracy required depends on problem type. For example, taut systems may require greater precision because Eqs. 2.4a~2.4b operate along a steeper envelope as the line becomes stretched.

Although the partitioned solution technique requires a greater number of iterations to converge onto a solution, a reduction of the function evaluations can be achieved by computing the inner-loop Jacobians using Eqs. 4.16/4.17. Moreover, the matrix pattern for the inner-loop Jacobian permits the matrix to be inverted without resorting to factorization methods. These improvements can be applied to the original work in [28] to augment both speed and accuracy of the partitioned method. Unlike the monolithic approach, the partitioned strategy avoids the need for matrix reordering, which is required with the monolithic MSQS technique since zero entries lie on the diagonal of Eq. 4.7. By virtue of Eq. 4.2:

$$(6.1) \quad \frac{\partial \{F_{Z_i}\}}{\partial Z_i} = 0$$

With the monolithic approach demonstrated in this manuscript, matrix re-ordering is necessary to eliminate the diagonal zeros in the  $\mathbf{A}$  matrix block.

The benefit of the monolithic approach is that the Jacobian is computed entirely analytically to enable both loose and tight coupling within the FAST simulation tool. The partitioned solution approach demonstrated in [28] is challenging to implement in this framework since the outer-loop Jacobians must be computed numerically (using finite-difference) and that internal state variables are present. The force-balance derivatives can be obtained analytically with the monolithic approach because  $H_i$  and  $V_i$  are constant in Eq. 4.2 within nonlinear iterations. With the partitioned approach,  $H_i$  and  $V_i$  change within the outer-loop iteration. Because  $H_i$  and  $V_i$  cannot be expressed as closed form solutions, the outer-loop Jacobian must be computed numerically.

Improvements were added to the monolithic MSQS strategy to increase robustness and accuracy. The improvements focus on the relative magnitude between the  $\mathbf{A}$  and  $\mathbf{C}$  matrix blocks. The matrix condition number for  $\mathbf{J}$  is decreased by changing the units in which the problem is solved in. For underwater mooring systems, [kN] is an appropriate unit scale; however, for smaller systems, such as cable-driven parallel robots [10], [N] units would be appropriate. An additional scaling factor was included to reduce the relative size of the diagonal entries in  $\mathbf{J}$ . Benefits of the scaling factor become increasingly more important for cable systems that combine different line properties, different segment lengths, and include both taut and slack moorings.

Finally, this paper also highlights the process used to derive the closed-form analytical solution to the catenary equation with the condition of a cable in contact with the seabed. This condition is an important ingredient to solve practical problems commonly arising in offshore mooring systems. Historical precedent has been limited to using a discretized cable, such as a lumped-parameter model, to address the cable/seabed contact problem. This paper presents a new technique to address this issue.

#### REFERENCES

- [1] R. ADREZIN, P. BAR-AVI, AND H. BENAROYA, "Dynamic Response of Compliant Offshore Structures – Review", *J. Aerospace Engineering*, 9(4):114–131, 1996.

- [2] V. AGRAWAL, W. J. PEINE, B. YAO, AND S. CHOI, “Control of Cable Actuated Devices using Smooth Backlash Inverse”, IEEE International Conference on Robotics and Automation, Anchorage, AK, May 2010.
- [3] API RP 2SK, *Design and Analysis of Stationkeeping System for Floating Structures, Third Edition*, American Petroleum Institute, 2005.
- [4] API RP 2SM, *Recommended Practice for Design, Manufacture, Installation, and Maintenance of Synthetic Fiber Ropes for Offshore Mooring, Third Edition*, American Petroleum Institute, 2001.
- [5] L. M. BERGDAHL, AND I. RASK, “Dynamic vs. Quasi-Static Design of Catenary Mooring Systems”, Offshore Technology Conference, Paper No. 5530, Houston, TX, April 27–30, 1987.
- [6] J. BROWN, M. G. KNEPLEY, D. A. MAY, L. C. MCINNES, AND B. F. SMITH, “Composable Linear Solvers for Multiphysics”, 11<sup>th</sup> International Symposium on Parallel and Distributed Computing (ISPD 2012), June 25–29, Munich, Germany, 2012.
- [7] Y. T. CHAI, K. S. VARYANI AND N. D. P. BARLTROP, “Semi-Analytical Quasi-Static Formulation for Three-Dimensional Partially Grounded Mooring System Problems”, *Ocean Engineering*, 29:627–649, 2002.
- [8] I. CORBETTA, AND F. SLOAN, “HMPE Mooring Line Trial for Scarabeo III”, Offshore Technology Conference”, Paper No. 13272”, Houston, TX, April 30 – May 3, 2001.
- [9] J. GOBAT, THE DYNAMICS OF GEOMETRICALLY COMPLIANT MOORING SYSTEMS, Ph.D. Thesis. Massachusetts Institute of Technology and Woods Hole Oceanographic Institute, 2000.
- [10] C. GOSSELIN AND S. BOUCHARD, “A Gravity-Powered Mechanism for Extending the Workspace of a Cabledriven Parallel Mechanism: Application to the Appearance Modelling of Objects”, *J. Automation Technology*, 4(4):372–379.
- [11] S. INGRAM, “Minimum Degree Reordering Algorithms: A Tutorial”, University of British Columbia, 2013.
- [12] E. R. JEFFERYS AND M. H. PATEL, “On The Dynamics of Taut Mooring Systems”, *Engineering Structures*, 1(4):37–43, 1982.
- [13] J. M. JOHNSEN, AND O. ØRITSLAND, “Design and Optimization of Taut-Leg Mooring Systems”, Offshore Technology Conference”, Paper No. 10776, Houston, TX, May 3–6, 1999.
- [14] J. M. JONKMAN AND M. L. BUHL, *FAST User’s Guide*, NREL Technical Report, NREL/EL-500-38230, Golden, CO, 2005.
- [15] J. M. JONKMAN, *Dynamics Modeling and Loads Analysis of an Offshore Floating Wind Turbine*, National Renewable Energy Laboratory, Technical Report NREL/TP-500-41958, November, 2007.
- [16] B. J. JONKMAN, J. M. MICHALAKES, J. M. JONKMAN, M. BUHL, A. PLATT, AND M. A. SPRAGUE, *NWTC Programmer’s Handbook: A Guide for Software Development within the FAST Computer-Aided Engineering Tool (DRAFT)*, NREL Technical Report, NREL/TP-xxxx-xxxx, Golden, CO, 2012.
- [17] J. JONKMAN, “The New Modularization Framework for the FAST Wind Turbine CAE Tool”, 51<sup>st</sup> AIAA Aerospace Sciences Meeting,
- [18] K. KOZAK, W. ZHOU, AND W. JINSONG, “Static Analysis of Cable-Drive Manipulators With Non-Negligible Cable Mass”, *IEEE Transactions on Robotics*, 22(3):425–433, 2006.
- [19] M. IRVINE, *Cable Structures*, Dover Publications, Mineola, NY, 1992.
- [20] I. LIIV, “Seriation and Matrix Reordering Methods: An Historical Overview”, *Statistical Analysis and Data Mining*, 3(2):70–91, 2010.
- [21] M. MASCIOLA, N. NAHON AND F. R. DRISCOLL, “Static Analysis of the Lumped Mass Cable Model using a Shooting Algorithm”, *J. Waterway, Port, Coastal, and Ocean Engineering*, 138(2), 2012.
- [22] M. MASCIOLA, J. JONKMAN, AND A. ROBERTSON, “Implementation of a Multisegmented, Quasi-Static Cable Model”, International Ocean (Offshore) and Polar Engineering Conference, June 30 – July 5, Anchorage, AK, 2013.
- [23] B. B. MEKHA, C. P. JOHNSON AND J. M. ROESSET, “Implications of Tendon Modeling on Nonlinear Response of TLP”, *J. Structural Engineering*, 122(2):142–149, 1996.
- [24] J. J. MORÉ, B. S. GARBOW, AND K. E. HILLSTROM, *User Guide for MINPACK-1*, Argonne National Laboratory, Report No. ANL-80-74, 1980.
- [25] W. MUSIAL, AND B. RAM, “Large-Scale Offshore Wind Power in the United States,” National Renewable Energy Laboratory Technical Report NREL/TP-500-49229, September, 2010.
- [26] J. NOCEDAL AND Y. YUAN, “Combining Trust Region and Line Search Techniques”, Northwestern University, Department of Electrical Engineering and Computer Science, 1992.
- [27] B. PAUL AND A. SOLER, “Cable Dynamics and Optimum Towing Strategies for Submersibles”, Offshore Technology Conference, Houston, TX, may 2–5, 1972.
- [28] A. H. PEYROT AND A. M. GOULOUS, “Analysis of Cable Structures”, *Computers & Structures*,

- 10:805–813, 1979.
- [29] S. QUALEN, T. XING, P. CARRICA, Y. LI AND J. XU, “CFD Simulation of a Floating Offshore Wind Turbine System Using a Quasi-Static Crowfoot Mooring-Line Model”, Twenty-third International Offshore and Polar Engineering, June 30–July 5, Anchorage, AK, 2013.
  - [30] S. E. RAMBERG AND O. M. GRIFFIN, “Free Vibrations of Taut and Slack Marine Cables”, *J. of the Structural Division*, 108:1662–1662, 1977.
  - [31] Y. SAAD *Iterative Methods for Sparse Linear Systems, Second Edition*, Society for Industrial and Applied Mathematics, Philadelphia, PA, 2003.
  - [32] B. SKAARE, T. D. HANSON, F. G. NIELSEN, R. YTTTERVIK, A. M. HANSEN, K. THOMSEN, AND T. J. LARSEN, “Integrated Dynamic Analysis of Floating Offshore Wind Turbines”, European Wind Energy Conference and Exhibition, 2007.
  - [33] R. E. SKELTON AND M. C. DE OLIVEIRA, “*Tensegrity Systems*”, Springer, New York, NY, 2009.
  - [34] K. VESLIĆ, “Finite Catenary and the Method of Lagrange”, *Society for Industrial and Applied Mathematics*, 37(2), 1995.
  - [35] H. F. VELDKAMP AND J. VAN DER TEMPEL, “Influence of Wave Modeling of the Prediction of Fatigue for Offshore Wind Turbines”, *Wind Energy*, 5:46–65, 2005.
  - [36] R. WEBSTER, “On the Static Analysis of Structures with Strong Geometric Nonlinearity”, *Computers & Structures*, 11, 1980.
  - [37] P. WILLIAMS AND P. TRIVAILA, “Dynamics of Circularly Towed Cable Systems, Part 1: Optimal Configurations and Their Stability.”, *J. of Guidance, Control, and Dynamics*, 30(2):753–765, 2007.
  - [38] J. F. WILSON, *Dynamics of Offshore Structures*, John Wiley & Sons, Hoboken, NJ, 2003.